Applied Catalysis A, General 623 (2021) 118242

Contents lists available at ScienceDirect

Applied Catalysis A, General

journal homepage: www.elsevier.com/locate/apcata

The nickel-support interaction as determining factor of the selectivity to ethylene in the oxidative dehydrogenation of ethane over nickel oxide/alumina catalysts

Yousra Abdelbaki [a,d], Agustín de Arriba [a], Benjamín Solsona [b,*], Daniel Delgado [a,e], Ester García-González [c], Rachid Issaadi [d], José M. López Nieto [a,*]

[a] Instituto de Tecnología Química, Universitat Politècnica de València-Consejo Superior de Investigaciones Científicas, Avenida de los Naranjos s/n, 46022, Valencia, Spain
[b] Departament d'Enginyeria Química, Universitat de València, C/ Dr. Moliner 50, 46100, Burjassot, Valencia, Spain
[c] Departamento Química Inorgánica, Facultad de Ciencias Químicas, Universidad Complutense, 28040, Madrid, Spain
[d] Hydrogen Energy Applications Laboratory, Faculty of Technology, University of Blida 1, Algeria
[e] Department of Inorganic Chemistry, Fritz-Haber-Institute of the Max-Planck-Gesellschaft, 14195, Berlin, Germany[1]

ARTICLE INFO

Keywords:
Ethylene
Oxidative dehydrogenation of ethane
ODH
Nickel oxide
Alumina
Catalyst characterization (XPS, HREM, UV raman and UV–vis-DRS)

ABSTRACT

Nickel oxides supported on γ-alumina (Ni-loading from 5 to 30 wt% NiO) have been synthesized and tested in the oxidative dehydrogenation (ODH) of ethane in order to determine the importance of the NiO-support interaction. The best performance was achieved by the catalyst with 15 wt% NiO; higher NiO-loadings lead to the formation of unselective bulk-like NiO and lower Ni-loadings present high proportion of free alumina surface sites. The presence of oxalic acid and/or niobium in the synthesis gel resulted in the formation of NiO particles with similar size, but higher crystallinity and reducibility than the standard 15 wt% NiO catalyst. The obtained results have revealed that, in addition to NiO crystal size, the nickel oxide-support interaction determines the catalytic performance of these catalysts.

1. Introduction

The recent discovery of shale gas reserves has caused a decrease in the price of natural gas, encouraging its use as feedstock for the production of valuable chemicals [1]. Ethylene is, by far, the most important chemical feedstock for Petrochemistry, being directly used in the production of a wide number of commodity chemicals [2]. Currently, the main industrial route to obtain ethylene is steam cracking, which is an energy intensive and non-catalytic process [2,3]. In fact, steam cracking is considered as the most energy consuming process of the chemical industry, due to its endothermic character and the need for high reaction temperatures. Moreover, the absence of catalysts leads to the formation of many reaction products so that the separation costs are also high. Among all the possibilities, the oxidative dehydrogenation (ODH) of ethane is established as one of the most interesting alternatives to steam cracking, being an exothermic process with lower energy requirements and no thermodynamic limitations [3–5]. The energy consumption of ODH is expected to be substantially lower than any of the current alkene production technologies due to its exothermic nature. Furthermore, the deposition of coke is prevented provided that the presence of oxygen can oxidize coke to form carbon oxides. Despite the large amount of research efforts, industrial scale application of the ODH of ethane has not been implemented up to date due to the relatively low ethylene selectivity shown by the catalysts currently available. The main problem with most of the catalysts studied for the ODH of ethane is the excessive formation of carbon oxides (CO_x) which limits the selectivity to ethylene [3–6]. In this sense, among all catalytic systems based on reducible metal oxide catalysts, the most promising ones are multicomponent MoV(Te,Sb)NbO mixed oxides [7,8] and modified NiO materials [9–21]. In the latter case, it has been reported that pure NiO exhibits an important formation of CO_2 and low ethylene selectivity [9–20]. However, the role of promoters [9–15] and/or supports/diluents [16–25] in NiO based catalysts is still under discussion. In this way, several investigations have shown the effect of different promoters on

* Corresponding author.
E-mail addresses: benjamin.solsona@uv.es (B. Solsona), jmlopez@itq.upv.es (J.M. López Nieto).
[1] Present address.

https://doi.org/10.1016/j.apcata.2021.118242
Received 16 April 2021; Received in revised form 26 May 2021; Accepted 3 June 2021
Available online 6 June 2021

the catalytic behavior of NiO-based materials [9–25], with the presence of many promoters reducing the formation of carbon dioxide. Nevertheless, at this moment, Nb-promoted catalysts are the most effective ones [9–15], although the presence of other elements, such as Sn^{4+}, W^{6+}, Zr^{4+}, Ti^{4+} [10–15], with dopant contents lower than 10 at.%, favor small changes in the characteristics of NiO particles, thus leading to the best catalytic performance (selectivity to ethylene up to 80–90 %).

Alternatively, supported/diluted NiO catalysts also show a high ethylene selectivity, especially by using Al_2O_3 [16–19], porous clays [20] or other supports based on transition metal oxides [21–25]. In this case, after the incorporation of NiO contents of ca. 10−30 wt%, changes in both physico-chemical characteristics and catalytic performance are observed. These changes have been related to a decrease in crystal size of NiO particles but, in addition, some interaction between NiO and the support (decreasing the reducibility of Ni-O bonds) could be also necessary. Thus, it is known that the decrease of the NiO crystallite size [9,21], the elimination of non-stoichiometric oxygen species, a decrease in the reducibility of Ni^{n+} sites, an increased Lewis acidity [15,26,27] or a lower electron conductivity [28] can give rise to high selectivity to ethylene during the ODH of ethane [9,11,12,17]. Interestingly, a similar increasing effect in the selectivity to the olefin in the ODH of ethane has been observed when oxalic acid is incorporated during the preparation procedure [15].

Generally, nickel oxide catalysts with small NiO particle size (below 20 nm, although less than 10 nm is preferred) present optimum catalytic performance in the ODH of ethane [15]. However, the drastic change observed in the redox properties of NiO must rely on the modification of the chemical nature of NiO (coordination, surface environment, oxidation state) [9,15]. This could be achieved by decreasing NiO particle size. However, it is possible to increase the selectivity to ethylene by optimizing the active phase-support interaction, without substantially decreasing NiO particle size, as observed in TiO_2-supported nickel oxide catalysts [28]. Thus, and according to these observations, it seems that a small particle size might not be a sufficient requirement to improve the catalytic performance of NiO-based catalysts in ODH.

In order to shed some light into the chemical nature of selective NiO catalysts for the oxidative dehydrogenation of ethane, we have synthesized Al_2O_3-supported nickel oxide catalysts, but with varying degrees of nickel oxide-support interaction by using modifying the catalyst preparation procedure. In this way, it will be possible to determine the influence of the interaction between nickel oxide and the support, minimizing the possible interference of both the NiO crystal size effect and the support employed.

Accordingly, we have followed two different synthetic approaches for a series of NiO/Al_2O_3 catalysts: i) addition of oxalic acid as an organic additive to NiO/Al_2O_3 system; and ii) incorporation of Nb^{5+} as a dopant during the preparation of the Al_2O_3-supported materials. In the latter case, the synthesis of Nb^{5+}-promoted NiO/Al_2O_3 catalysts has been carried out by incorporating Nb^{5+} in one or two steps: a) using a Ni^{2+}/Nb^{5+}-containing solution to be directly impregnated on Al_2O_3; and b) Nb^{5+} is firstly impregnated on Al_2O_3, and a Ni^{2+}-containing solution is subsequently added on the NbO_x-Al_2O_3 support. The results are discussed in terms of the specific chemical and structural features found in selective and unselective materials.

2. Experimental

2.1. Catalysts preparation

Al_2O_3-supported NiO catalysts were prepared by wet impregnation of γ-Al_2O_3 (S_{BET} =210 m^2/g, ABCR) with aqueous solutions of nickel nitrate $Ni(NO_3)_2{\cdot}6H_2O$ (Sigma-Aldrich, 99 %). The catalysts are named as **xNi/AL**, where x is the NiO wt%.

Alternatively, oxalic acid was added to the nickel nitrate solution, with Ni/oxalic acid molar ratios of 1/1 and 1/3 (i.e. **15Ni/AL-o1** and **15Ni/AL-o3** catalysts, respectively). For comparison, a 15 NiO wt% Al_2O_3 catalyst was prepared by a mechano-chemical procedure, by mixing and grinding the corresponding amounts of nickel oxide and alumina in an agate mortar (i.e. **Ni+AL(PM)** sample).

Nb-containing alumina-supported nickel oxide catalysts were prepared by following two strategies, using an aqueous solution of $C_4H_4NNbO_9{\cdot}xH_2O$ (Sigma–Aldrich): i) direct impregnation of γ-Al_2O_3 by an aqueous solution of promoting compounds and subsequent impregnation with an aqueous solution of nickel nitrate (15 wt% NiO) named as **Ni/Nb/AL**; ii) γ-Al_2O_3-supported Ni-Nb-O mixed oxides were prepared by wet impregnation method using aqueous solutions of nickel nitrate and the niobium compound, with a Nb/(Ni + Nb) atomic ratio of 0.1; which has been named as **(Ni+Nb)/AL**. All catalysts were dried overnight at 100 °C and finally calcined at 500 °C for 2 h (5 °C/min). The characteristics of these catalysts are shown in Table 1.

2.2. Catalytic tests

Catalytic tests were carried out under steady state conditions in a fixed bed quartz reactor (i.d. 20 mm, length 400 mm) at temperatures in the 300−500 °C range. Feed consisted of an ethane/O_2/He mixture with 3/1/26molar ratio. The total flow and the catalyst weight were varied (25−100 mL min^{-1}, 0.1–1.0 g of catalyst and 0.3–0.5 mm particle size) in order to achieve several contact times (W/F). For some selected experiments an ethane/O_2/He mixture with 3/3/24molar ratio was employed.

Reactants and products were analyzed by gas chromatography using two packed columns [20]: (i) molecular sieve 5A (2.5 m); and (ii) Porapak Q (3 m).

2.3. Catalysts characterization

N_2-adsorption isotherms were recorded in a Micromeritics ASAP 2000 device. The materials were degassed in vacuum at 300 °C prior to N_2 adsorption. Surface areas were estimated by the Brunauer-Emmet-Teller (BET) method.

X-ray diffraction patterns were collected in an Enraf Nonius FR590 diffractometer with a monochromatic $CuK_{\alpha 1}$ source operated at 40 keV and 30 mA.

Raman spectra were obtained in an inVia Renishaw spectrometer, equipped with an Olympus microscope, using a wavelength of 325 nm (UV-Raman), generated with a Renishaw HPNIR laser with a power of approximately 15 mW.

UV–vis diffuse reflectance spectroscopy measurements of the solids were carried out within the 200−800 nm range using a *Varian* spectrometer model Cary 5000. The value of band gap Eg is calculated by extrapolating the linear fitted region at $[F(R(\infty))h\upsilon]^2 = 0$ in the plot of $[F(R(\infty))\ h\upsilon]^2$ versus $h\upsilon$. Additional information in supporting information.

Temperature-programmed reduction experiments (H_2-TPR) were performed in an Autochem 2910 (Micromeritics) equipped with a TCD detector. The reducing gas composition was 10 % H_2 in Ar, with a total flow rate of 50 mL min^{-1}. The materials were heated until 800 °C, with a heating rate of 10 °C min^{-1}.

X-ray photoelectron spectroscopy (XPS) measurements were performed on a SPECS spectrometer equipped with a Phoibos 150 MCD-9 detector using a monochromatic Al Kα (1486.6 eV) X-ray source. Spectra were recorded using an analyzer pass energy of 50 eV, an X-ray power of 100 W, and an operating pressure of 10^{-9} mbar. Spectra treatment was performed using CASA software. Binding energies (BE) were referenced to C *1s* at 284.5 eV.

Selected area electron diffraction (SAED), high-resolution transmission electron microscopy (HRTEM) and Scanning-TEM (STEM)-Energy-Dispersive Spectroscopy (EDS) maps were performed on a JEOL JEM300 F electron microscope by working at 300 kV (point resolution of 0.17 nm). Crystal-by-crystal chemical microanalysis was performed by energy-dispersive X-ray spectroscopy (XEDS) in the same microscope

Table 1
Characteristics of catalysts and their catalytic results in the ODH of ethane.

Catalyst	NiO (wt.%)	S_{BET} (m^2 g^{-1})	TPR (H_2-uptake) [e]	Eg (eV) [f]	Ethane conversion (%)	Selectivity to ethylene (%)	Selectivity to ethylene (%)[g]	Catalytic activity [h]	Catalytic Activity/NiO [i]	STY rate of product formation [j]
5Ni/AL	5	202	17	4.50	0.92	88	88	14.6	293	13.7
10Ni/AL	10	189	49	4.08	1.2	94.7	88	19.1	191	16.7
15 Ni/AL	15	171	71	3.81	3.4	95.0	93	54.1	361	47.3
20 Ni/AL	20	166	86	3.70	4.4	91.5	90	70.1	350	59.8
30 Ni/AL	30	152	126	3.60	7.7	70.9	72	123	409	81.1
Ni/Nb/AL	15	151	77	3.58	2.1	78.6	71	33.4	223	24.5
(Ni+Nb)/AL	15	184	63	3.50	4.5	88.5	86	71.6	478	59.2
15Ni/AL-o1[b]	15	195	50	3.25	6.8	78	78	108	722	78.8
15Ni/AL-o3[c]	15	195	72	3.55	5.3	63.6	63	84.4	563	50.1
Ni+AL (PM) [d]	15	173	65	3.48	8.6	39.4	39	137	913	50.4

[a] At 400ºC and a contact time, W/F, of 20.5 g_{cat} h mol^{-1}_{C2H6} ; [b] Oxalic acid/nickel molar ratio in synthesis gel of 1; [c] Oxalic acid/nickel molar ratio in synthesis gel of 3; [d] mechano-chemical mixture; [e] hydrogen-uptake during the TPR experiments, in mL_{H2}/g_{cat}; [f] Edge energy in eV, determined from DR-UV–vis spectra; [g] Selectivity to ethylene at 400ºC and isoconversion of 10 %; [h] Catalytic activity (in g_{C2H6} kg^{-1}_{cat} h^{-1}); [i] Catalytic activity per loading of NiO (in g_{C2H6} kg^{-1}_{NiO} h^{-1}); [j] Space-time yield, STY, is the formation rate of ethylene (in g_{C2H4} kg^{-1}_{cat} h^{-1}).

equipped with an ISIS 300 X-ray microanalysis system (Oxford Instruments) with a detector model LINK "Pentafet" (resolution 135 eV). Samples for transmission electron microscopy (TEM) were ultrasonically dispersed in n-butanol and transferred to carbon coated copper grids.

3. Results and discussion

3.1. Catalytic results in the ODH of ethane

The catalytic performance of supported nickel oxide catalysts during the oxidative dehydrogenation (ODH) of ethane at 400 °C is summarized in Table 1. As mentioned in the experimental section, the catalysts tested consist of a set of nickel oxide materials supported on γ-alumina, with Ni-loadings from 5 to 30 wt% NiO. In addition, catalysts with a 15 wt% NiO prepared with different amounts of oxalic acid and promoted with Nb^{5+} were also evaluated.

The ethane conversion and the selectivity to ethylene strongly depend on NiO-loading and the catalyst preparation procedure. For comparison, it has been also included the catalytic results of a mechano-chemical NiO-Al_2O_3 mixture, named as **Ni+AL(PM)**. In all cases, ethylene was the main reaction product. In addition, CO_2 was the only product detected from oxidation reactions.

The variation of the selectivity to ethylene with the ethane conversion during the ethane ODH on representative Al_2O_3-supported nickel oxide catalysts (xNi/AL series) is shown in Fig. 1a. On the other hand, Fig. 1b allows the comparison of catalytic results over catalysts with 15 wt% NiO with or without additional synthetic modifications: i) Nb-promoted catalysts, i.e. **Ni/Nb/AL** and **(Ni+Nb)/AL** samples; ii) unpromoted catalysts prepared from synthesis gels containing oxalic acid (i.e. **15Ni/AL-o1** and **15Ni/AL-o3** samples).

As it can be observed in Fig. 1a and Table 1, the selectivity to ethylene has a clear dependence on the NiO-loading. Thus, the selectivity to ethylene gradually increases with NiO-loading (in the range of 88–95 %), reaching a maximum of ca. 95 % over sample **15Ni/AL** (i.e. 15 wt% NiO). On the contrary, further increasing NiO-loading on Al_2O_3 (up to 30 wt% NiO) leads to a decrease in the selectivity to ethylene during the ODH of ethane (down to ca. 72 %).

In the case of Nb-promoted catalysts, the **(Ni+Nb)/AL** sample (synthesized in one step) presents a slight decrease in the selectivity to ethylene (ca. 86 %) compared to that achieved using the reference sample, **15Ni/AL**. Moreover, **Ni/Nb/AL** catalyst (prepared in two steps) presents a remarkably lower selectivity (ca. 71 %).

The method used to prepare the catalysts, and especially the presence of oxalic acid in the synthesis gel, may also have an important influence in the catalytic performance. Fig. 1b shows the variation of selectivity with ethane conversion of samples with 15 wt% of NiO. Lower selectivity to ethylene is observed over samples prepared with oxalic acid in the synthesis gel (see **15Ni/AL-o1** and **15Ni/AL-o3**), especially notorious when high oxalic acid contents are used. Thus, both Nb-promoted NiO/γ-Al_2O_3 catalysts and Nb-free NiO/γ-Al_2O_3 catalysts

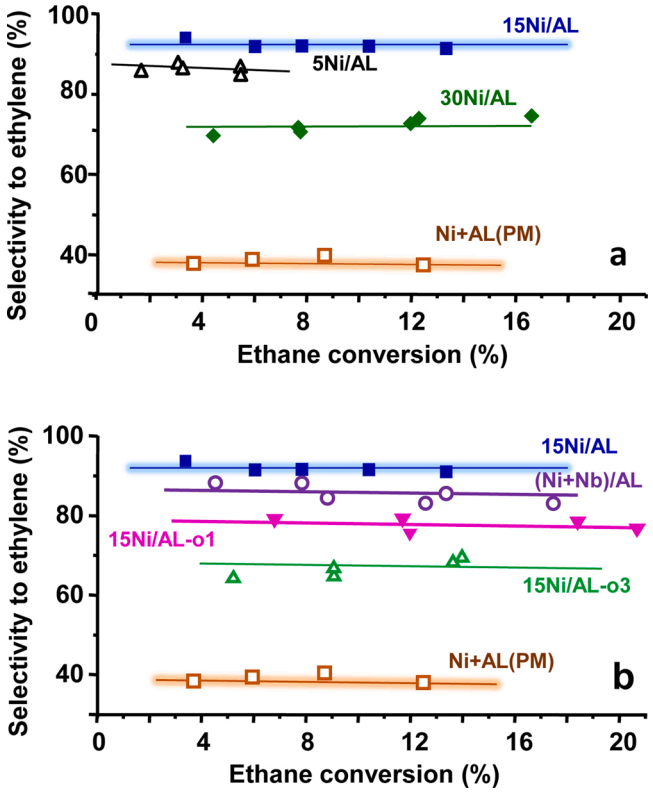

Fig. 1. Variation of the selectivity to ethylene with the ethane conversion on: a) xNi/AL series; and b) on catalysts with 15 wt% NiO, with or without additional synthetic modifications. Note: reaction conditions in the main text, reaction temperature 400-450 °C. Catalysts: **5Ni/AL** (△); **15Ni/AL** (■); **30Ni/AL** (♦); **15Ni/AL-o1** (▼); **15Ni/AL-o3** (△); **(Ni+Nb)/AL** (○). Data corresponding to the mechano-chemical mixture, **Ni+AL(PM)** (□), have been included for comparison.

(where the oxalic acid has been directly added) show a poorer selectivity to ethylene than the corresponding catalyst of xNi/Al series (i.e. **15Ni/AL** sample). The selectivity to ethylene for catalysts prepared with a 15 wt% NiO decreases according to the following trend: **15Ni/AL** > **(Ni+Nb)/AL** > **15Ni/AL-o1** > **Ni/Nb/AL** > **15Ni/AL-o3** > **Ni+AL (PM)**.

Fig. 2 shows the variation of the space-time yield for ethylene formation of studied catalysts. For xNi/AL series, the formation of ethylene per nickel site increases with the NiO-loading, achieving its maximum value for **20Ni/AL** catalyst (Fig. 2). However, the highest space-time yield for ethylene formation was observed for samples **15Ni/AL-o1** and **(Ni+Nb)/AL** (Fig. 2). This is so because of the higher C_2H_6 reaction rates for the latter cases (Figure S1, supporting information).

The present study has been undertaken using a low concentration of oxygen ($C_2H_6/O_2/He$ = 3/1/26 M ratio) so achieving high conversions without running out of oxygen is complicated. Then, we have carried out a few experiments with the optimal catalyst **15Ni/AL** using more oxygen in the feed ($C_2H_6O_2/He$ = 3/3/24) and higher contact times to reach higher conversions. Thus, an ethane conversion of 51.2 % and a selectivity to ethylene of 71.7 %, so that the ethylene yield obtained was 36.7 %, was obtained when working at 450 °C and a contact time, W/F, of 205 g_{cat} h $(mol_{C2H6})^{-1}$ (Table S1, supporting information). This yield could be enhanced by optimizing the reaction conditions.

3.2. Characterization of Al_2O_3-supported nickel oxide catalysts

In order to understand their catalytic performance, the catalysts were characterized by several physicochemical techniques. Table 1 summarizes their main physicochemical characteristics. Fig. 3 displays the XRD patterns of Al_2O_3-supported NiO catalysts synthesized in the absence or the presence of increasing amounts of oxalic acid or Nb-oxalate in the synthesis gel. For comparison, XRD pattern of the mechano-chemically mixed **Ni+AL(PM)** sample is presented in Figure S2-A (supporting information).

All the materials show diffraction lines corresponding to face-centered cubic NiO phase, space group Fm-3m (JCPDS: 78−0643), and γ-alumina (JCPDS: 10−0425). However, depending on the catalyst preparation procedure (the NiO-loading and/or the presence/absence of Nb^{5+} as promoter), differences in the relative intensity of diffraction maxima of the two crystal phases were observed. X-ray diffraction patterns of the catalysts from xNi/AL series show a progressive increase in the relative intensity of NiO diffraction maxima as the nickel oxide loading increases (see Fig. 3, patterns *a* to *e*). For the same nickel oxide content (we have considered the optimal Ni/Al ratio), the incorporation of increasing amounts of oxalic acid leads to an increase in the relative intensity of the NiO peaks (Fig. 3, diagrams *c*, *h* and *i*).

Likewise, both the use of niobium as a promoter and the method

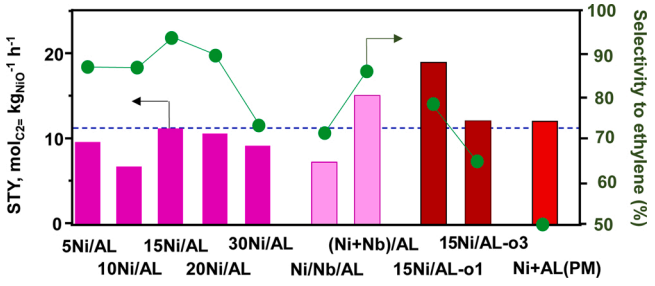

Fig. 2. Variation of the space time yield ethylene formation rate per nickel oxide site (vertical bars) on NiO/Al_2O_3 catalysts of the xNi/AL series and catalysts with 15 wt% NiO with additional synthetic modifications. Reaction conditions: 400 °C, different contact times and $C_2/O_2/He$ = 3/1/26 M ratio. Variation of selectivity to ethylene at an ethane conversion of 10 % (reaction temperature, 400 °C) (●). Note: Selectivity of **Ni + AL(PM)** is very low (ca. 39 %).

followed to incorporate it, modify the relative intensity and peak width of NiO maxima, for a fixed Ni/Al content (again, we have considered the optimal NiO content of 15 wt%). Thus, NiO diffraction maxima appear to be narrower in **Ni/Nb/AL** sample than in **(Ni+Nb)/AL** (Fig. 3, patterns *f* and *g*, respectively), which could be related to differences in NiO crystal size and/or degree of crystallinity, depending on the extent of interaction with γ–Al_2O_3 support.

In order to get further insight into the crystalline nature of NiO-based catalysts, these materials were analyzed by high-resolution transmission electron microscopy. Catalysts of the xNi/AL series are made up of γ–Al_2O_3 and NiO crystallites of 5−10 nm in size up to the composition **15Ni/AL**, NiO showing a good dispersion over the support (Figs. 4a and 4b). In the **20Ni/AL** catalyst, platelet-like NiO crystals of 30−50 nm begin to appear (Fig. 4c), which are very abundant, and in the form of agglomerates in **30Ni/AL** sample (Fig. 4d).

The addition of oxalic acid tends to modify the microstructure of the catalysts. After adding oxalic acid in 1:1 Ni/oxalic acid molar ratio (catalyst **15Ni/AL-o1**), crystallinity, the degree of dispersion on the support and the average size of the NiO crystallites, remain almost unchanged with respect to that observed in catalyst **15Ni/AL.** However, for 1: 3 Ni/oxalic acid molar ratio (i.e. **15Ni/AL-o3** sample), NiO particles display higher crystallinity, even though the average crystallite size hardly changes (Fig. 4e). Note that despite the similarity between X-ray patterns of **15Ni/AL-o3** and **30Ni/AL** catalysts (Fig. 3, patterns *i* and *e*, respectively), their microstructure is quite different.

In the case of niobium promoted catalysts, microstructural differences are found depending on the preparation method. The Nb-promoted $NiO/\gamma\text{-}Al_2O_3$ catalyst prepared in two steps (**Ni/Nb/AL** sample) is formed by NiO crystallites of 10−15 nm distributed on the support, as well as agglomerates of large crystals of ~ 50 nm. EDS maps (Figure S3) show a homogeneous distribution of niobium on the $\gamma\text{-}Al_2O_3$ support and the absence of niobium in areas where NiO crystals are observed. Interestingly, well-dispersed crystallites of approximately 5−10 nm size with a characteristic *d* spacing of approximately 7 Å can be also observed in this catalyst. Provided the chemical composition of the sample and the elemental distribution, this periodicity is compatible with the (002) *d* spacing of Ni_2O_3 (d_{002} = 7.29 Å). These crystallites are clearly visible in Fig. 4f. It is important to mention that this is the only catalyst in which this type of crystals have been observed, and the details of the preparation method in this particular case must be the origin of the formation of this species.

For Nb-promoted $NiO/\gamma\text{-}Al_2O_3$ prepared in one step, **(Ni+Nb)/AL**, NiO crystallites of 10−15 nm distributed on the support with agglomerates of larger NiO crystals of ~ 50 nm were observed. These large crystals are less abundant than in the catalyst prepared in two steps. EDS maps performed (Figure S4) show that, although in low concentration, niobium is effectively distributed and associated with nickel on the support.

Al_2O_3-supported NiO catalysts were also characterized by UV Raman spectroscopy (using an excitation wavelength of 325 nm) in order to elucidate the spin-phonon interaction in the materials [29,30]. Fig. 5 shows the UV Raman spectra of alumina-supported nickel oxide catalysts. For comparison, the UV Raman spectrum of **Ni+AL(PM)** sample is presented in Figure S2 (pattern B).

As reported in the literature, the UV Raman spectra of bulk NiO are characterized by the presence of five Raman bands [29,30]: i) two bands at ca. 510 and 580 cm^{-1}, assigned to one-phonon (1P) transverse optical (*TO*) and longitudinal optical (*LO*) modes; ii) two weak bands at ~740 cm^{-1} and ~900 cm^{-1} and an intense band at ca. 1100 cm^{-1} related to two-phonon modes, i.e. the second-order transverse optical mode (*2TO*), the combination of *TO* + *LO* modes and the second-order longitudinal optical (*2LO*) modes, respectively. Among all these bands, the most intense ones are those located at 580 and ca. 1100 cm^{-1}.

We must notice that, when NiO is antiferromagnetically ordered or defect-rich, the intensity of one-phonon scattering (1P, *LO* and *TO* modes) increases significantly [29,31]. In addition, a very low intensity

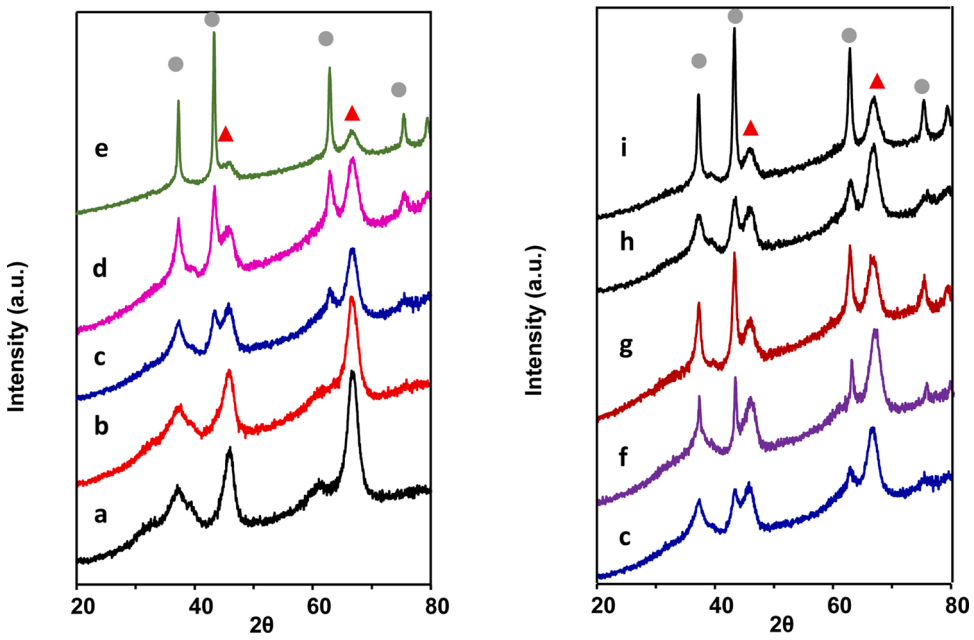

Fig. 3. XRD patterns of Al_2O_3-supported NiO catalysts: a) **5Ni/AL**; b) **10Ni/AL**; c) **15Ni/AL**; d) **20Ni/AL**; e) **30Ni/AL**; f) **Ni/Nb/AL**; g) **(Ni+Nb)/AL**; h) **15Ni/AL-o1**; i) **15Ni/AL-o3**. Diffraction lines of NiO (●) and γ-Al_2O_3 (▲) have been marked.

of the band at ca. 1124 cm^{-1} has been observed in silica-supported nickel oxide (with 3 wt% NiO), which has been attributed to the presence of very small NiO crystals [32]. In addition, the presence of only one band at ca. 570 cm^{-1} has been recently reported for NiO supported on Nb^{5+}-containing siliceous porous clay heterostructure catalysts [33]. This observation was attributed to a high NiO dispersion as a consequence of an effective active phase-support interaction, what would lead to a decrease in NiO particle size and/or the generation of defects.

As expected, the intensity of the most characteristic bands (1P *LO* band at ~580 cm^{-1} and 2P *2LO* band at ~1100 cm^{-1}) increases when the nickel oxide loading increases (Fig. 5). However, the relative growth of both bands differs depending on the specific structural and chemical features of the catalyst. Thus, an increase in the intensity of 2P *2LO* band (I_{1100}) higher than that of 1P *LO* band (I_{580}) is observed at high NiO-loading. Therefore, the relative intensity of 1P *LO* band simultaneously increases with the decrease of NiO particle size and/or the presence of oxygen defects [31]. This fact would mean that the increase in the nickel oxide loading favors an increase of the NiO crystal size and/or a decrease in the concentration of oxygen defects.

UV Raman spectra of catalysts with the same NiO-loading (with or without Nb^{5+} or oxalic acid in the synthesis gel) are comparatively shown in Fig. 5 (spectra *c*, *f* to *i*). Differences are observed in the relative intensity of the *LO* band (I_{580}) and *2LO* band (I_{1100}) depending on the catalyst preparation procedure. Catalysts **15Ni/AL** and **(Ni+Nb)/AL** present an I_{580}/I_{1100} ratio higher than 1; whereas **Ni/Nb/AL**, **15Ni/AL-o1** and **15Ni/AL-o3** catalysts present I_{580}/I_{1100} ratios lower than 1. These results could be partly explained in terms of the presence of NiO particles with different crystal sizes. However, the distribution and the mean crystal size of NiO in the reference catalyst (**15Ni/AL**) and sample **15Ni/AL-o1** are very similar, despite being the relative I_{580}/I_{1100} ratio much higher in the reference catalyst.

In the same way, Nb-promoted NiO/Al_2O_3 catalysts prepared in either one or two synthesis steps (**(Ni+Nb)/AL** and **Ni/Nb/AL**, respectively) also present significant differences in their UV Raman profiles (Fig. 5, spectra *f* and *g*, respectively). Despite showing similar NiO crystal size, both catalysts display different relative I_{580}/I_{1100} ratio, being higher in the material prepared in one-step (i.e. **(Ni+Nb)/AL** sample). In addition, this would also underline the low capability of niobium oxide in the dispersion of NiO [34].

The DR-UV–vis spectra of prepared catalysts are shown in Fig. 6, in which spectra *a* to *e* correspond to Al_2O_3-supported NiO catalysts with different Ni-loadings, while spectra *f* to *i* are those corresponding to catalysts prepared in the presence of oxalate anions, Nb-promoted and unpromoted catalysts. For comparison, DR-UV–vis spectrum of NiO-Al_2O_3 mixture, **Ni+AL(PM)** sample, has been also recorded (Figure S2-C).

Bulk NiO shows bands at 715 nm and 377 nm, which can be assigned to octahedrally coordinated Ni^{2+} species in the NiO lattice [17,19,23,35,36]. Additionally, a band at 510 nm can be also assigned to charge transfer in NiO crystals [36,37]. On the other hand, it has been reported that supported nickel oxide catalysts, such as NiO-Al_2O_3 [38,39], NiO/Silica-Alumina [39] or NiO/Al_2O_3 [17,19], can also present a doublet (at 600–645 nm) and a band at 416–430 nm, which were attributed to Ni^{2+} species with tetrahedral (Td) and octahedral (Oh) coordination, respectively. Nevertheless, a band at 630 nm has been also observed in NiO supported on TiO_2/γ-Al_2O_3 [40], which has been attributed to the absorption of surface-dispersed nickel oxide species in tetrahedral coordination. We must note that the accommodation of Ni^{2+} species in both tetrahedral and octahedral coordination could lead to nickel aluminate as surface spinel phase in samples calcined at higher temperatures [17,24,36,38–40].

According to our results, the DR-UV–vis spectra of samples of xNi/AL series with NiO-loading up to 10 wt% NiO suggest the presence of Ni^{2+} species with tetrahedral (doublet at 600 and 640 nm) and octahedral (band at 410 nm) coordination, without the appearance of the band at 715 nm, typical of bulk NiO (Fig. 6 a–b). These results could indicate the existence of highly dispersed nickel species with high interaction between support and part of Ni-containing crystallites (Ni^{2+} tetrahedral diffused into the γ-Al_2O_3 lattice) [17,24,36,38,39]. At this point it is important to mention that $NiAl_2O_4$ spinel was not detected neither by X-ray diffraction nor by electron microscopy. When nickel loading increases, the interaction with the support reaches a maximum (15 wt% NiO or below), and from there, NiO crystals begin to grow, reaching larger size. Then, the bands corresponding to Ni^{2+} in octahedral coordination in NiO begin to be observed in the spectrum of the **15Ni/AL** catalyst, thus indicating the simultaneous presence of nickel sites linked to the support as well as bulk NiO (Fig. 6, spectra c–e). The above analysis is in strong agreement with what was observed by electron

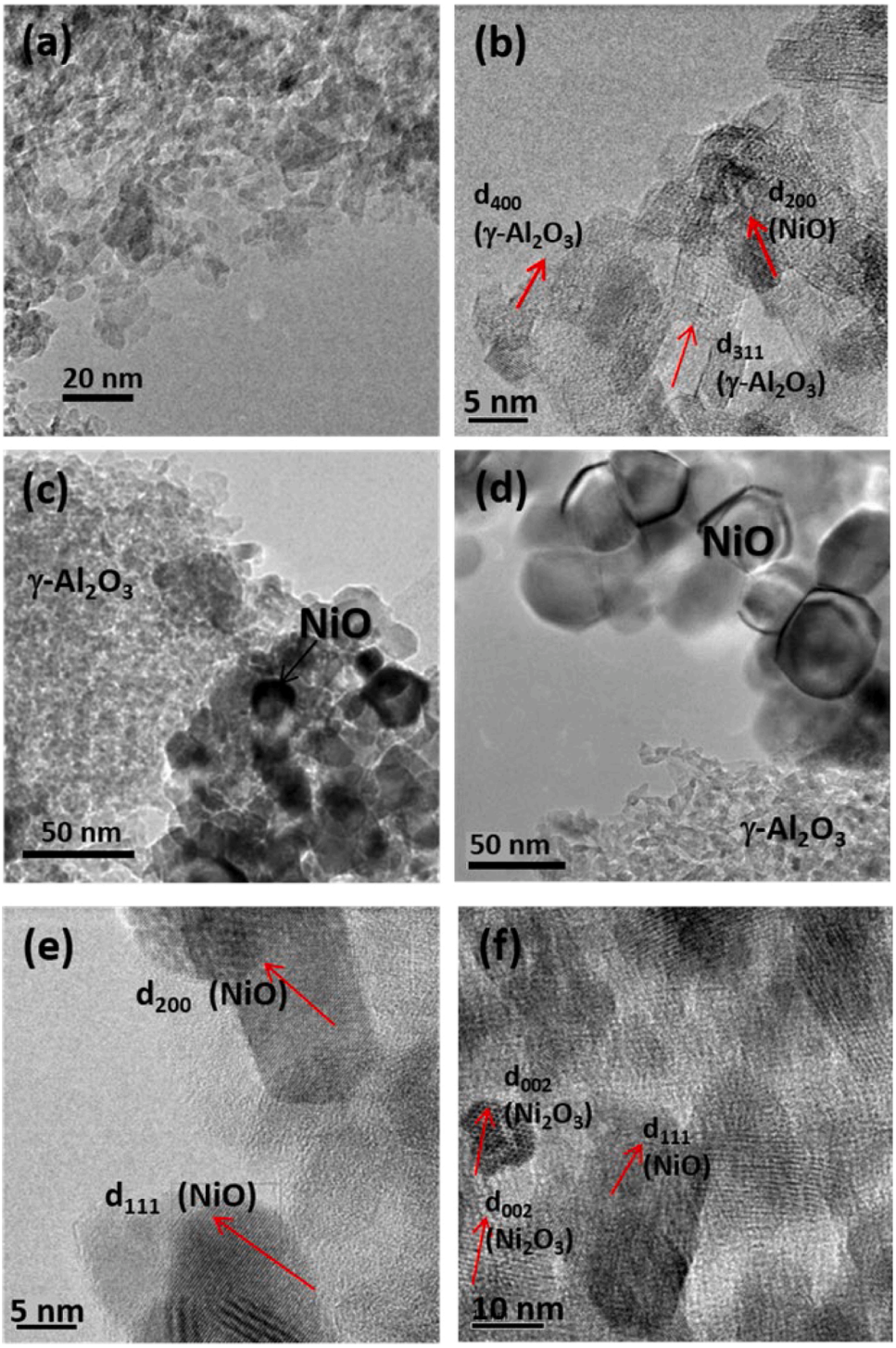

Fig. 4. High resolution transmission electron micrographs corresponding to crystallites of catalysts: **15Ni/AL** (a and b), **20Ni/AL** (c), **30Ni/AL** (d), **15Ni/AL-o3** (e), and **Ni/Nb/AL** (f).

microscopy, where NiO crystals of 5−10 nm size are observed in **10Ni/AL** and **15Ni/AL**, in the last one co-existing with agglomerates of larger polygonal NiO crystals.

In Nb-promoted catalysts, the nature of Ni^{2+}-species depends on the catalyst preparation procedure. Spectrum of **Ni/Nb/AL** sample shows an intense band at 715 nm, Ni^{2+}(Oh), in addition to a small band at 630 nm, Ni^{2+}(Td) (Fig. 6, spectrum g). Thus, the presence of niobium species on the surface of support, as in the **Ni/Nb/AL** catalyst, limits the NiO-support interaction, thus favoring NiO crystallization. However, the distribution of niobium associated to nickel in **(Ni+Nb)/AL** sample (one-step synthesis), limits the growth of NiO crystals as the band at 715 nm shows lower intensity (Fig. 6, spectrum *f*). Accordingly, agglomerates of large NiO crystals are more abundant in **Ni/Nb/AL** sample, as observed by electron microscopy.

Bands corresponding to NiO at 377 and 715 nm are particularly intense in catalysts **15Ni/AL-o1** and **15Ni/AL-o3**, indicating that crystallized NiO has a weak interaction with the support. This fact is in agreement with electron microscopy data, where an increase in the crystallinity of NiO is observed although the size of the crystallites does not increase significantly.

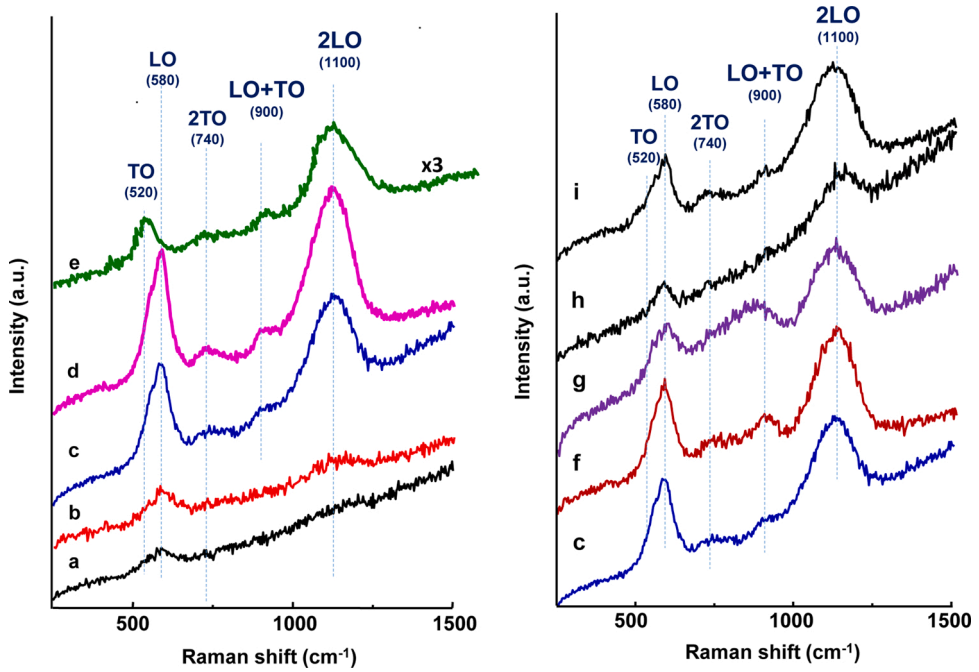

Fig. 5. UV-Raman spectra of Al_2O_3-supported NiO catalysts: a) **5Ni/AL**; b) **10Ni/AL**; c) **15Ni/AL**; d) **20Ni/AL**; e) **30Ni/AL**; f) **(Ni+Nb)/AL**; g) **Ni/Nb/AL**; h) **15Ni/AL-o1**; i) **15Ni/AL-o3**.

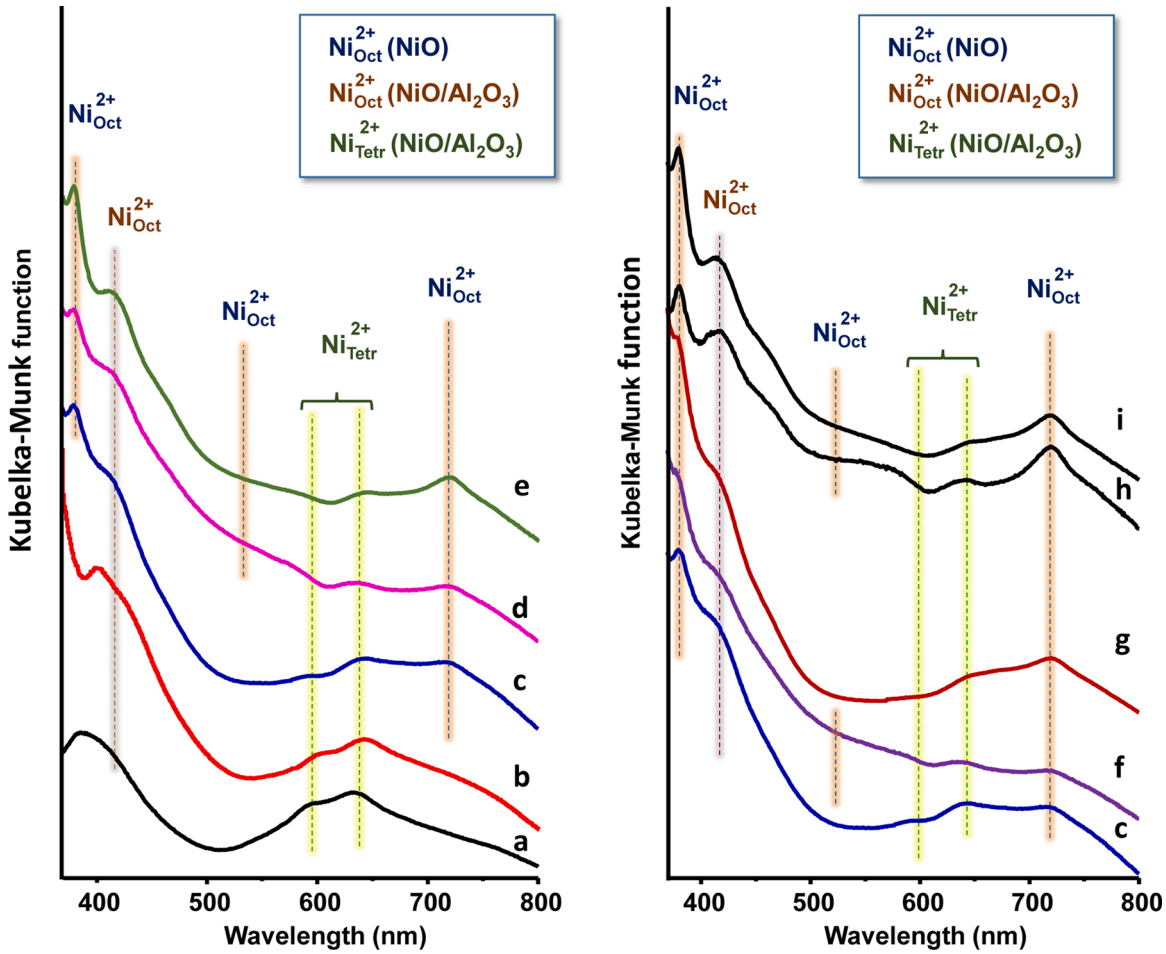

Fig. 6. Diffuse reflectance UV–vis spectra of Al_2O_3-supported NiO catalysts: a**) 5Ni/AL**; b) **10Ni/AL**; c) **15Ni/AL**; d) **20Ni/AL**; e) **30Ni/AL**; f) **(Ni + Nb)/AL**; g) **Ni/Nb/AL**; h) **15Ni/AL-o1**; i) **15Ni/AL-o3.**

Table 1 summarizes the energy band gaps (E_g, in eV) of supported nickel oxide catalysts calculated from Kubelka-Munk function (Figure S5). In general, E_g values decrease when increasing the Ni-loading. In the same way, for a fixed NiO loading (15 wt%), the lowest band gap values are observed in Nb-containing catalysts (3.50 and 3.58 eV) and catalysts prepared in the presence of oxalic acid in the synthesis gel (3.25 and 3.55 eV). Samples from xNi/AL series with NiO contents in the range 5−15 wt% display the highest E_g among the samples analyzed (4.05−3.81 eV) (Table 1), which are also the most selective catalysts in the ODH of ethane. In our case, small differences are observed for all the catalysts, however, these band gap values alone cannot explain their catalytic properties as it may be influenced by various factors such as crystallite size, structural parameter, carrier concentrations, presence of impurities and lattice strain [41–44].

In order to study the reducibility of catalysts and NiO-support interaction, TPR-H_2 experiments were performed. Fig. 7 shows the TPR-H_2 profiles of xNiO/AL catalysts with different NiO-loading (Fig. 7, patterns *a* to *e*) and catalysts with 15 wt% NiO, with or without promoters, and synthesized by different preparation procedures (Fig. 7, patterns *f* to *i*). For comparative purposes, TPR-H_2 profile of a mechanochemical mixture, **Ni+AL(PM)** sample (Fig. S2), is also included.

The shape of reduction profiles depends on the strength of NiO-support interaction. In the prepared catalysts, profiles show three main features corresponding to (in order of decreasing reduction temperature) (Fig. 7): i) the reduction of small and highly dispersed NiO particles for which the above interaction is strong [17–19,36], which gives a peak at ca. 520−550 °C (observed in all catalysts); ii) the reduction of NiO particles that tend to form small agglomerates with medium strength interaction with the support, that originates a reduction peak slightly above 450 °C (observed in sample with Ni-loading of 15 wt%); and iii) the reduction of large NiO crystals with weak interaction with the support, which gives a peak at ca. 340 °C, similar to that observed in pure NiO [17–25] (observed in sample **30Ni/AL**).

Additionally, differences in reducibility can be clearly observed as a function of the catalyst preparation procedure when comparing catalysts with 15 wt% NiO (Fig. 7, patterns *c*, *f-i*). In this sense, Nb-promoted catalysts show a peak of high reducibility at 330 °C, which is more intense and constitutes the main feature of the reduction profile in **Ni/Nb/AL**. On the other hand, **(Ni+Nb)/AL** catalyst shows lower reducibility, with the main peak appearing at 530 °C. These results are consistent with the structural characterization. Thus, higher reducibility of Ni-species in **Ni/Nb/AL** catalyst can be interpreted on the basis of a low interaction between NiO and support (NbO_x/Al_2O_3), which facilitates the growth of crystals and the formation of agglomerates that are more easily reduced. In this way, it has been proposed that Nb_2O_5 has not shown good properties as a NiO diluter/support, being unable in these conditions to eliminate a large proportion of non-selective sites [34].

In catalysts prepared with oxalic acid in the synthesis gel, the reduction profiles show a unique peak around 400−450 °C, in contrast with the xNi/AL series with Ni-loading below 15 wt% NiO, that presents a reduction peak at ca. 520 °C. According to TEM data, catalysts with 15 wt% of NiO and different amounts of oxalic acid (i.e. **15Ni/AL-o1** and **15Ni/AL-o3**) present a similar size distribution of the NiO crystals, although crystallinity clearly improves compared to **15Ni/AL** when increasing amounts of oxalic acid are used. A poor interaction with the support is the reason of this change as well as the decrease in reducibility. This is also in agreement with results from DR-UV–vis spectra.

It is worth mentioning that nickel aluminate-like species present a reduction peak at ~ 800 °C, as reported in the literature [17,38]. This peak is not observed in the reduction profiles of the catalysts under study. This is in agreement with the structural and microstructural characterization of the samples, where the formation of $NiAl_2O_4$ has not been observed in any case. However, the possible presence of this phase cannot be completely ruled out, although, if present, it should be in low concentration in samples with low NiO-loading.

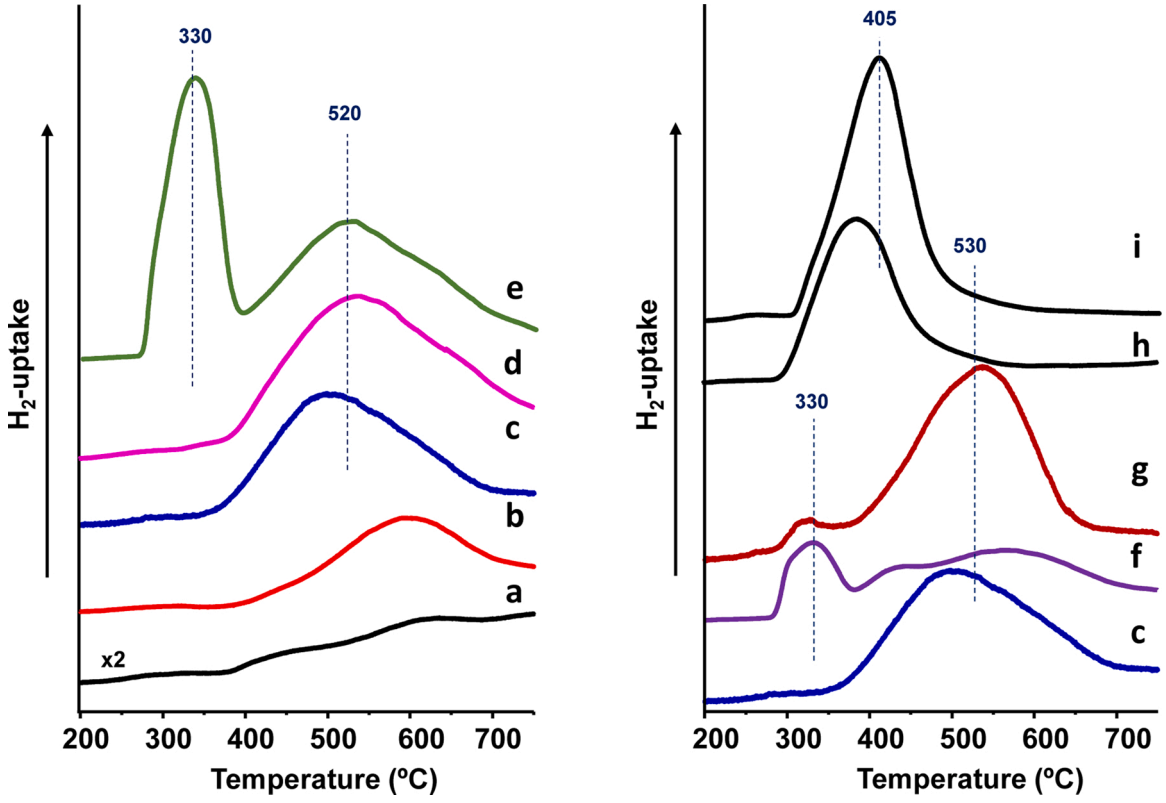

Fig. 7. TPR-H_2 profiles of Al_2O_3-supported NiO catalysts: a) **5Ni/AL**; b) **10Ni/AL**; c) **15Ni/AL**; d) **20Ni/AL**; e) **30Ni/AL**; f) **Ni/Nb/AL**; g) **(Ni+Nb)/AL**; h) **15Ni/AL-o1**; i) **15Ni/AL-o3**.

According to the TPR-H_2 experiments (Fig. 7), the catalyst **15Ni/AL** presents the highest NiO-support interaction among the samples with a Ni-loading of 15 wt% NiO, also showing the maximum relative intensity of LO (1 P) band in UV Raman spectra (Fig. 5).

Fig. 8 shows Ni $2p_{3/2}$ core-level XPS spectra for selected Al_2O_3-supported NiO catalysts, whereas Figures S4 and S5 displays the XPS results of additional NiO-based materials. Ni $2p_{3/2}$ core level spectra present the characteristic features of NiO, i.e. a main peak (ca. 856 eV) together with two satellites at 1.5–2.0 and 7.0 eV over the main peak (Sat I and Sat II, respectively) [13,15,33]. Sat I can be attributed to the presence of a wide variety of defects, such as Ni^{2+} vacancies, Ni^{3+} species or surface Ni^{2+}-OH species; while Sat II is usually assigned to ligand-metal charge transfer. Changes in the relative intensity of Sat I signal have been related to the variations in the concentration of defects or in the particle size, which can be favored when an effective NiO-support interaction takes place [9,15,17–21,33]. Unfortunately, not a clear relationship between the relative intensity of Sat I / Main peak and the selectivity to ethylene has been observed.

O *1s* core level spectra are shown in Fig. 9 and Figure S6. In general, the O *1s* signal of alumina appeared at higher binding energy (532.2 eV) than the signal for nickel oxide (530.5 eV) in all cases, as seen elsewhere [45]. The contribution of the alumina O *1s* signal is bigger for the catalysts with Ni-loading lower than 20 wt% (Fig. 9), with a symmetric display of the peak. However, a shift of the band to lower binding energy is observed for catalysts with 30 wt% of NiO (Fig. S6), samples prepared with Nb (especially for **Ni/Nb/AL** sample (Fig. 9)) or a mechano-chemically treated sample (Fig. S6), in agreement with a worst dispersion of the NiO. A strong interaction of the oxygen anions with the Ni^{2+} cations for these catalysts was also suggested as a shift to lower binding energy occurred.

Al *2p* and Ni *3p* spectra for the catalysts with different Ni amount (Fig. 10), show a single peak at 74.8 eV for Al *2p*, corresponding to the Al^{3+} species in octahedral coordination, together with a signal at 68.5 eV, attributed to Ni *3p* core level [45]. This latter Ni *3p* core level peak increases in intensity as the NiO-loading increases. On the other hand, a small shift to lower binding energies when increasing the Ni loading is observed, likely associated with a progressively higher interaction of Al^{3+}-bonded oxygen sites with Ni^{2+} cations, resulting in a distortion of the Al_2O_3 octahedral network [45].

In Nb *3d* XPS spectra (Fig. S7), Nb-containing catalysts presented a classical doublet with a split spin-orbit of the components of 2.78 eV which is related to the unique presence of dispersed Nb^{5+} [33].

3.3. A determining factor of the selectivity to ethylene

The TPR experiments undertaken confirm the close relationship between reducibility of nickel oxide species and the interaction of NiO particles with the support, which seems to determine the selectivity to ethylene during ethane ODH. Fig. 11 plots the relative hydrogen consumption of the band at 330 °C (reduction degree), related to NiO with low interaction with the alumina support, and the selectivity to ethylene at isoconversion conditions. It can be observed that the presence of NiO with low interaction with the alumina support must be avoided in order to achieve high ethylene formation, since an inverse relationship between the hydrogen consumption of the NiO reduction peak and the selectivity to the olefin has been observed. Accordingly, a higher interaction between NiO particles and support decreases the reducibility of Ni^{n+} species, and the concentration of electrophilic oxygen species, thus favoring a more controlled oxygen supply during catalytic cycles, and a higher selectivity to the olefin.

This NiO-support interaction determines not only NiO crystal size, but also the definition/crystallinity of the crystals (and the concentration of defects in the active phase). As discussed in the UV Raman spectra, an increase in the relative intensity of the 1 P LO band (I_{580}) with respect to that for 2 P 2LO band (I_{1100}) means that the NiO crystallite size decreases and/or the amount of oxygen defects increases. As the crystal size in all the catalysts is not constant, an accurate estimation of the number of defects cannot be undertaken through this technique. Interestingly, as observed by TEM, the reference catalyst **15Ni/AL** and those with oxalic acid (samples **15Ni/AL-o1** and **15Ni/AL-o3**) present very similar NiO crystal size (Fig. 4). However, the I_{580}/I_{1100} ratio in the corresponding UV Raman spectrum of **15Ni/AL** (Fig. 5, spectrum *c*) is remarkably higher than that observed for **15Ni/AL-o1** and **15Ni/AL-o3** catalyst (Fig. 5, spectra *h* and *i*). Accordingly, a different concentration of oxygen species can be proposed for the reference catalyst (**15Ni/AL**).

Similarly, both Nb-containing catalysts present similar NiO crystal

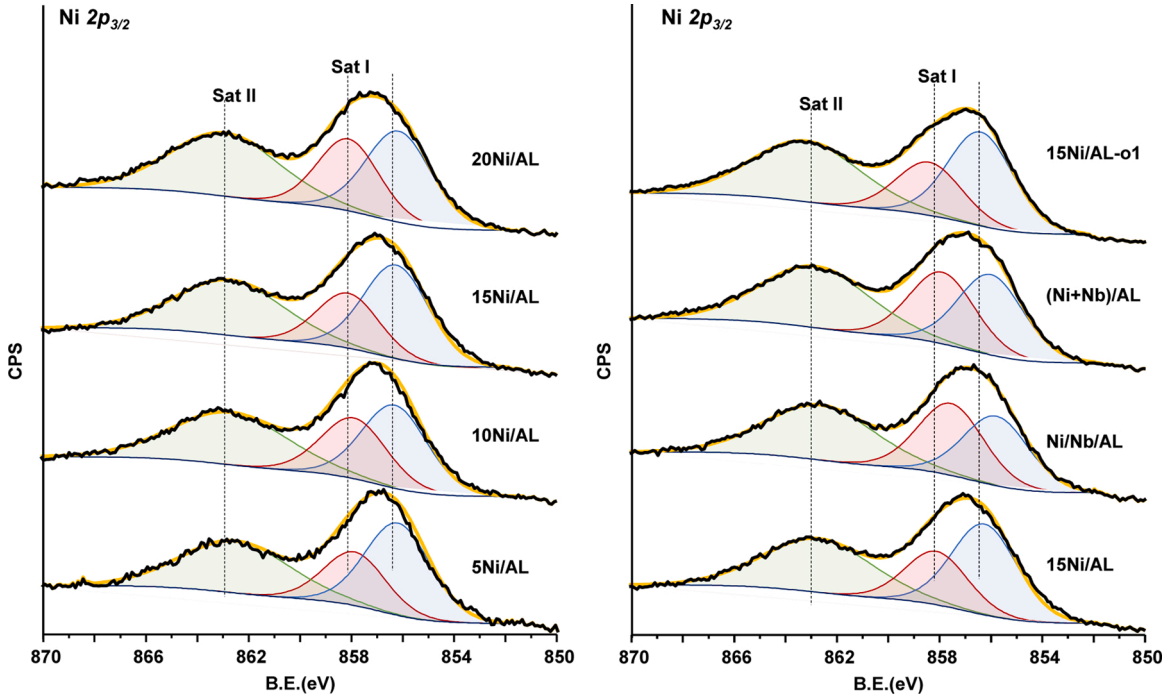

Fig. 8. Ni $2p_{3/2}$ core-level XPS spectra: xNi/Al catalysts (left); selected Al_2O_3-supported NiO catalysts with 15 wt% NiO (right).

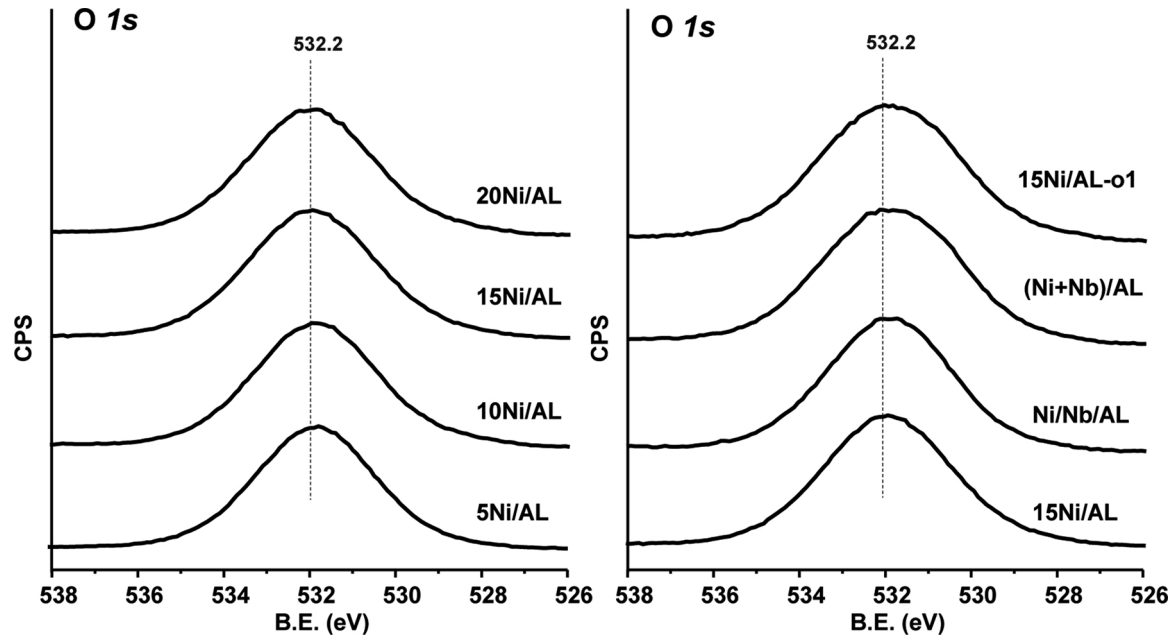

Fig. 9. O *1s* core-level XPS spectra of supported nickel oxide catalysts: xNi/Al catalysts (left); selected Al_2O_3-supported NiO catalysts with 15 wt% NiO (right).

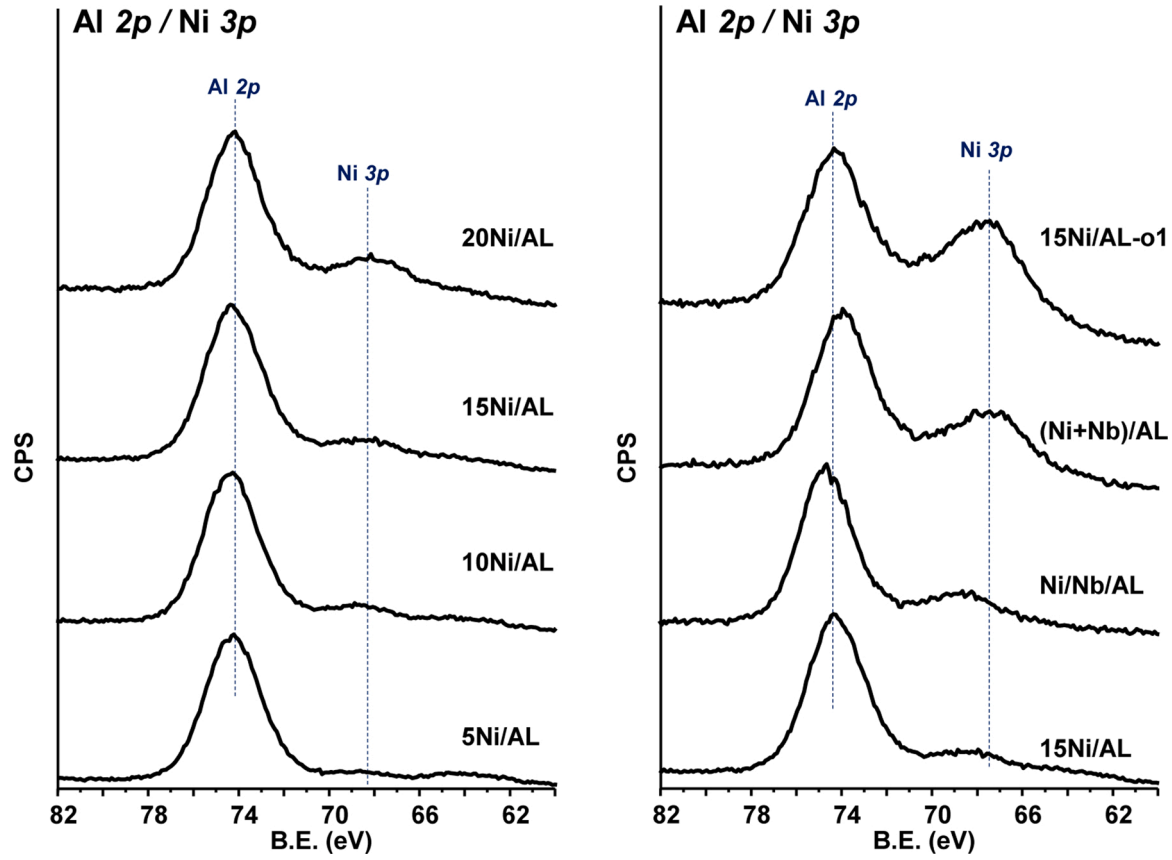

Fig. 10. Al *2p* and Ni *3p* core-level XPS spectra: xNi/Al catalysts (left); selected Al_2O_3-supported NiO catalysts with 15 wt% NiO (right).

size (Fig. 4), but the catalyst prepared in one step **(**Ni+**Nb)/AL** displays a higher I_{580}/I_{1100} ratio in the corresponding UV Raman spectra than the one prepared in two steps (**Ni/Nb/AL**) (Fig. 5, spectra *f* and *g*), which also results in a higher ethylene selectivity.

4. General remarks

Al_2O_3-supported nickel oxide catalysts prepared by a conventional wet impregnation method (without oxalic acid in the synthesis gel) showed high selectivity to ethylene during the ethane ODH. In this way, catalysts with NiO-loadings of 15–20 wt% NiO display interesting

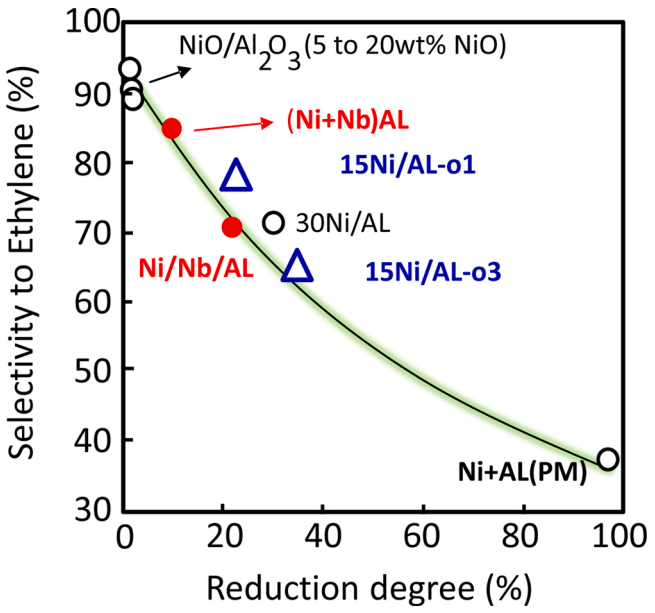

Fig. 11. Relationship between the selectivity to ethylene during the ethane ODH and the reduction degree (calculated from the TPR peak at ca. 330 °C). Reaction conditions for ethane ODH in text, 10 % ethane conversion, reaction temperature 400-450 °C.

catalytic properties (with a selectivity to ethylene higher than 90 %), in agreement with previous results from other authors [16–19]. The slightly lower selectivity to ethylene observed in the catalysts with 5–10 wt% NiO could be related to the presence of highly dispersed Ni^{2+}(Td) species but also to available unselective alumina sites, which present poor catalytic activity under our reaction conditions. The lower selectivity to ethylene observed over catalysts with Ni-loading higher than 20 wt% NiO can be related to the presence of big crystals of NiO, as deduced from TEM (Fig. 4), UV Raman (Fig. 5) and DR-UV–vis (Fig. 6) spectra, with weak NiO-support interaction, presenting high reducibility (Fig. 7).

It is especially noteworthy that the positive effect of the incorporation of Nb^{5+} in unsupported Nb-promoted NiO catalysts, which has been widely reported in the scientific literature [9–15], is not observed in supported Nb-promoted NiO/Al_2O_3 catalysts, regardless of the preparation method. In fact, both **(Ni+Nb)/AL** and **Ni/Nb/AL** catalysts present lower selectivity to ethylene than that observed for Al_2O_3--supported NiO catalysts displaying a NiO-loading from 10 to 20 wt%. The characterization results of these catalysts, as well as those prepared in the presence of oxalic acid in the synthesis gel, clearly indicate the presence of NiO particles with low interaction with the support, whose reducibility and crystallinity increases when increasing the concentration of oxalic acid in the synthesis gel.

For Al_2O_3-supported nickel oxide catalysts, the presence of oxalic acid during the synthesis has a deleterious effect on the catalytic performance, i.e. the higher the amount of oxalic acid in the synthesis gel, the lower is the selectivity to ethylene. This observation can be interpreted in terms of an increase in the reducibility of Ni^{n+} sites due to a lower NiO-support interaction, which is not only related to crystallite size, but also to the crystallinity.

The addition of an organic additive, such as oxalic acid, in the synthesis gel, during the preparation of unsupported materials, could help to decrease NiO particle size, thus leading to a material with lower amount of electrophilic oxygen, as observed in bulk SnO_2-NiO catalysts [15]. However, the presence of a support can hinder the interaction of the organic additive with the active phase, due to a favored coupling between the additive and the support. This fact can lead, as in the case of NiO/Al_2O_3 system, to NiO particles presenting a bigger particle size and a higher crystallinity, even when high amounts of oxalic acid are used, thus leading to a lower selectivity to the olefin in the ODH of ethane. Moreover, this is in agreement with the characterization results by XRD, diffuse reflectance UV–vis and UV Raman.

On the other hand, from XPS results (Figs. 8–10), it can be concluded that the samples with low reducibility (i.e. samples of xNi/AL series with NiO-loading lower than 20 wt. %) present: i) the characteristic features of NiO (with band at ca. 856 eV) and two satellites, Sat I and Sat II (at 1.5–2.0 and 7.0 eV, respectively, over the main peak) [9,15,17–21,33]; ii) a bigger contribution of the alumina O1 s signal (according to a higher dispersion of NiO); and iii) a shift to lower binding energy in the Al *2p* + Ni *3p* signal, confirming also the interaction between NiO particles and Al_2O_3 support [45]. All of these characteristics suggest the correlation between the selectivity to ethylene and a higher and more effective $NiO\text{-}Al_2O_3$ interaction.

It must be noted that the amount of carbon detected on the catalysts after use is negligible. This positive aspect is due to the oxidative conditions employed since the possible coke formed is oxidized into carbon dioxide. Moreover, TPR experiments of representative used catalysts were undertaken. As it can be seen in Figure S8 the differences between the fresh and the used catalysts are hardly perceptible. Then, the most characteristic features that define a TPR assay: the hydrogen consumption, the onset temperature and the temperature for the maximum hydrogen consumption, seem to keep unaltered after the reaction.

5. Conclusions

A tight correlation has been found between the $NiO\text{-}Al_2O_3$ interaction (as concluded from H_2-TPR) and the selectivity to ethylene during the oxidative dehydrogenation of ethane on alumina-supported nickel oxide catalysts. This interaction depends not only on the NiO crystal size and Ni-loading, but also on the synthesis method employed. Interestingly, NiO crystals with similar size have shown remarkably different interactions with the support and, consequently, different levels of ethylene formation.

The preparation method has been shown to be of capital importance to synthesize selective catalysts. Then, the use of oxalic acid in the preparation of $NiO/\gamma\text{-}Al_2O_3$ catalysts leads to lower NiO-alumina interaction, higher crystallinity of NiO particles and, subsequently, to a lower selectivity to ethylene during the ethane ODH.

The presence of Nb^{5+} in alumina-supported Ni-Nb-O catalysts (i.e. **(Ni+Nb)/AL**) has not improved the selectivity to ethylene with respect to the corresponding Nb-free catalyst (i.e. **15Ni/AL**), in contrast with the positive effect reported in bulk NiO catalysts. Nevertheless, the alumina-supported Ni-Nb-O catalysts, also prepared in presence of oxalate anions, are more selective to ethylene than the corresponding Nb-free samples prepared with oxalic acid in the synthesis gel (i.e. **15Ni/AL-o1**) or than the nickel oxide supported on $NbOx/\gamma\text{-}Al_2O_3$ (i.e. **Ni/Nb/AL**). Therefore, the presence of oxalate anions in the synthesis gel hinders the interaction between NiO and $\gamma\text{-}Al_2O_3$, favoring the formation of supported NiO particles with high crystallinity.

CRediT authorship contribution statement

Yousra Abdelbaki, Investigation, Discussing, Writing - review & editing. **Agustín de Arriba**, Investigation, Discussing, Writing - review & editing. **Benjamín Solsona**, Supervision, Conceptualization, Validation, Writing - review & editing, Funding. **Daniel Delgado**, Investigation, Discussing, Writing - review & editing. **Ester García-González**, Investigation, Discussing, Writing - review & editing. **Rachid Issaadi**, Methodology, Investigation, **José M. López Nieto,** Supervision, Conceptualization, Writing - review & editing, Funding.

Declaration of Competing Interest

The authors declare that they have no known competing financial interests or personal relationships that could have appeared to influence

the work reported in this paper.

Acknowledgements

Authors would like to acknowledge the Ministerio de Ciencia, Innovación y Universidades in Spain through projects CRTl2018-099668-B-C21, MAT2017-84118-C2-1-R and PID2019-106662RB-C44 and Ministry of Higher Education and Scientific Research of Algeria for the National Exceptional Program for the fellowships. A.A. acknowledges Severo Ochoa Excellence Program for his fellowship (BES-2017-080329). EGG acknowledges Dr. E. Urones for the valuable assistance in the use of electron microscopy facilities as well as to the CNME (Spain).

Appendix A. Supplementary data

Supplementary material related to this article can be found, in the online version, at doi:https://doi.org/10.1016/j.apcata.2021.118242.

References

[1] S. Bilgen, E. Sarıkaya, J. Natural Gas. Sci. Eng. 35 (2016) 637–645.
[2] T. Ren, M. Patel, K. Blok, Energy 31 (2006) 425–451.
[3] Y. Gao, L. Neal, D. Ding, W. Wu, Ch. Baroi, A.M. Gaffney, F. Li, ACS Catal. 9 (2019) 8592–8621.
[4] J.M. López Nieto, Top. Catal. 41 (2006) 3–15.
[5] C.A. Gärtner, A. van Veen, J.A. Lercher, ChemCatChem 5 (2013) 3196–3217.
[6] J.T. Grant, J.M. Venegas, W.P. McDermott, I. Hermans, Chem. Rev. 118 (2018) 2769–2815.
[7] P. Botella, E. García-González, A. Dejoz, J.M. López Nieto, M.I. Vázquez, J. González-Calbet, J. Catal. 225 (2004) 428–438.
[8] P. Botella, A. Dejoz, M.C. Abello, M.I. Vázquez, L. Arrúa, J.M. López Nieto, Catal. Today 142 (2009) 272–277.
[9] E. Heracleous, A.A. Lemonidou, J. Catal. 237 (2006) 162–174.
[10] Z. Skoufa, E. Heracleous, A.A. Lemonidou, Catal. Today 192 (2012) 169–176.
[11] Z. Skoufa, G. Xantri, E. Heracleous, A.A. Lemonidou, Appl. Catal. A Gen. 471 (2014) 107–117.
[12] a) H. Zhu, D.C. Rosenfeld, M. Harb, D.H. Anjum, M.N. Hedhili, S. Ould-Chikh, J.-M. Basset, ACS Catal. 6 (2016) 2852–2866;
b) H. Zhu, H. Dong, P. Laveille, Y. Saih, V. Caps, J.-M. Basset, Catal. Today 228 (2014) 58–64.
[13] a) B. Solsona, P. Concepción, B. Demicol, S. Hernández, J.J. Delgado, J.J. Calvino, J.M. López Nieto, J. Catal. 295 (2012) 104–114;
b) D. Delgado, B. Solsona, A. Ykrelef, A. Rodríguez-Gomez, A. Caballero, E. Rodríguez-Aguado, E. Rodríguez-Castellon, J.M. López Nieto, J. Phys. Chem. C 121 (2017) 25132–25142.
[14] Z. Skoufa, E. Heracleous, A.A. Lemonidou, J. Catal. 322 (2015) 118–129.
[15] J.M. López Nieto, B. Solsona, R.K. Grasselli, P. Concepción, Top. Catal. 57 (2014) 1248–1255.
[16] X. Zhang, Y. Gong, G. Yu, Y. Xie, J. Mol. Catal. A Chem. 180 (2002) 293–298.
[17] E. Heracleous, A.F. Lee, K. Wilson, A.A. Lemonidou, J. Catal. 231 (2005) 159–171.
[18] J.L. Park, S.K. Balijepalli, M.D. Argyle, K.J. Stowers, Ind. Eng. Chem. Res. 57 (2018) 5234–5240.
[19] L. Smolakova, M. Kout, E. Koudelkova, L. Capek, Ind. Eng. Chem. Res. 54 (2015) 12730–12740.
[20] B. Solsona, P. Concepción, J.M. López Nieto, A. Dejoz, J.A. Cecilia, S. Agouram, M. D. Soriano, V. Torres, J. Jiménez-Jiménez, E. Rodríguez Castellón, Catal. Sci. Technol. 6 (2016) 3419–3429.
[21] D. Delgado, R. Sanchís, J.A. Cecilia, E. Rodríguez-Castellón, A. Caballero, B. Solsona, J.M. López Nieto, Catal. Today 333 (2019) 10–16.
[22] J.P. Bortolozzi, L.B. Gutierrez, M.A. Ulla, Appl. Catal. A 452 (2013) 179–188.
[23] J.L. Park, K.A. Canizales, M.D. Argyle, B.F. Woodfield, K.J. Stowers, Microp. Mesop. Mat. 293 (2020), 109799.
[24] Zh. Zhang, G. Zhao, Y. Liu, Y. Lu, Microp. Mesop. Mat. 288 (2019), 109609.
[25] J.S. Valente, M. Valle-Orta, H. Armendariz-Herrera, R. Quintana-Solorzano, P. del Angel, J. Ramirez-Salgado, J.R. Montiel-López, Catal. Sci. Technol. 8 (2018) 4070–4082.
[26] D. Delgado, R. Sanchis, B. Solsona, P. Concepción, J.M. López Nieto, Top. Catal. 63 (2020) 1731–1742.
[27] I. Popescu, Z. Skoufa, E. Heracleous, A. Lemonidou, I.-C. Marcu, Phys. Chem. Chem. Phys. 17 (2015) 8138–8147.
[28] R. Sanchis, D. Delgado, S. Agouram, M.D. Soriano, M.I. Vázquez, E. Rodríguez-Castellón, B. Solsona, J.M. López Nieto, Appl. Catal. A Gen. 536 (2017) 18–26.
[29] R.E. Dietz, G.I. Parisot, A.E. Meixner, Phys. Rev. B 4 (1971) 2302–2310.
[30] E. Aytan, B. Debnath, F. Kargar, Y. Barlas, M.M. Lacerda, J.X. Li, R.K. Lake, J. Shi, A.A. Balandin, Appl. Phys. Lett. 111 (2017), 252402.
[31] N. Mironova-Ulmane, A. Kuzmin, I. Steins, J. Grabis, I. Sildos, M. Pärs, J. Phys. Conf. Ser. 93 (2007), 012039.
[32] S. He, X. Zheng, L. Mo, W. Yu, H. Wang, Y. Luo, Mat. Res. Bull. 49 (2014) 108–113.
[33] E. Rodríguez-Castellón, D. Delgado, A. Dejoz, I. Vázquez, S. Agouram, J.A. Cecilia, B. Solsona, J.M. Lopez Nieto, Chem. Eur. J. 26 (2020) 9371–9381.
[34] D. Delgado, B. Solsona, R. Sanchis, E. Rodríguez-Castellón, J.M. López Nieto, Catal. Today 363 (2021) 27–35.
[35] F. Iova, A. Trutia, Opt. Mater. 13 (2000) 455–458.
[36] J.S. Yoon, M.B. Park, Y. Kim, D.W. Hwang, H.-J. Chae, Catalysts 9 (2019) 933.
[37] Y. Kathiraser, W. Thisartarn, K. Suttiumporn, S. Kawi, J. Phys Chem. C 117 (2013) 8120–8130.
[38] Z. Boukha, C. Jimenez-Gonzalez, B. de Rivas, J. Gonzalez-Velasco, J.I. Gutierrez-Ortiz, R. López Fonseca, Appl. Catal. B 158-159 (2014) 190–201.
[39] P. Kim, Y. Kim, H. Kim, I.K. Song, J. Yi, Appl. Catal. A 272 (2004) 157–166.
[40] J. Wang, L. Dong, Y. Hu, G. Zheng, Z. Hu, Y. Chen, J. Solid State Chem. 157 (2001) 274–282.
[41] M. Hashem, E. Saion, N.M. Al-Hada, H.M. Kamari, A.H. Shaari, Z.A. Talib, S. B. Paiman, M.A. Kamarudeen, Results Phys. 6 (2016) 1024–1030.
[42] M.N. Siddique, A. Ahmed, T. Ali, P. Tripathi, AIP Conf. Proc. 1953 (2018), 030027, https://doi.org/10.1063/1.5032362.
[43] P. Mallick, R. Biswal, P. Mallick, R. Biswal, Nanosci. Nanotech. 6 (2016) 59–61, https://doi.org/10.5923/j.nn.20160604.01.
[44] A. Manikandan, J.J. Vijaya, L.J. Kennedy, Physica E 49 (2013) 117–123.
[45] G. Garbarino, P. Riani, A. Infantes-Molina, E. Rodríguez-Castellón, G. Busca, Appl. Catal. A 525 (2016) 180–189.